On the resolution of triangular meshes

S. Danilov[1,2]

[1]Alfred Wegener Institute, Helmholtz Centre for Polar and Marine Research, Bremerhaven, Germany
[2]Jacobs University, Bremen, Germany

Key Points:

- Geometrical resolution of an equilateral triangular mesh is defined by the height of its triangles.
- Quadrilateral and triangular meshes with the same number of vertices have approximately the same resolution.

Corresponding author: Sergey Danilov, sergey.danilov@awi.de

Abstract

It is generally agreed that the resolution of a regular quadrilateral mesh is the side length of quadrilateral cells. There is less agreement on what is the resolution of triangular meshes, exacerbated by the fact that the numbers of edges or cells on triangular meshes are approximately three or two times larger than that of vertices. However, the geometrical resolution of triangular meshes, i.e. maximum wavenumbers that can be represented on such meshes, is a well defined quantity, known from solid state physics. These wavenumbers are related to a smallest common mesh cell (primitive unit cell), and the set of mesh translations that map it into itself. The wavenumbers do not depend on whether discrete degrees of freedom are placed on vertices, cells or edges. The resolution is defined by the height of triangles.

Plain Language Summary

Some models used in climate studies are formulated on triangular computational meshes. We discuss how to determine the smallest scales that are resolved on such meshes. They are referred to as a mesh resolution. The notion of mesh resolution is used to relate climate model components formulated on different meshes.

1 introduction

Several recent global ocean circulation models are formulated on unstructured triangular meshes (Wang et al. (2014), Danilov et al. (2017), Korn (2017)) or their dual, quasi-hexagonal meshes (Ringler et al. (2013)). Unstructured-mesh models are also widely used in coastal applications (see, e.g., Chen et al. (2003), Zhang et al. (2016), Fringer et al. (2006), Androsov et al. (2019)). Triangular and hexagonal meshes are also common in atmospheric modeling (see, e.g., Wan et al. (2013), Kühnlein et al. (2019), Skamarock et al. (2012), Gassmann (2013), Dubos et al. (2015)). A question often arises on how to compare their resolution to that of the models formulated on regular quadrilateral meshes. In contrast to quadrilateral meshes, the number of cell and the number of vertices differ by the factor of two on triangular meshes, which creates an ambiguity.

The concept of 'resolution' discussed here is a geometrical one, i.e. we are interested in the largest wavenumbers that characterize discrete data on a given triangular (or hexagonal) mesh. The geometrical resolution should not be mixed with the effective resolution, as in Soufflet et al. (2016), which characterizes the scales where dynamics are not affected by dissipation. These scales depend not only on the mesh, but also on the details of discretization and numerical algorithm. We will briefly touch the aspect of effective resolution as concerns the effect of various placement of discrete variables.

In fact, the question on the resolved wavenumbers is addressed in numerous textbooks on solid state physics (see e.g. Kosevich (2005)). This note only repeats the known answers as applied to modeling on triangular meshes.

The key concept is that of mesh translations that leave the mesh unchanged. They define a primitive unit cell (unit cell further), which is the smallest repeating element of the mesh. The invariance of mesh to these translations leads to a reciprocal lattice in wavenumber space, and wave vectors become defined up to translations along the reciprocal lattice. Section 2 introduces the notions of unit cell, reciprocal lattice, and the first Brillouin zone of triangular (hexagonal) mesh. The first Brillouin zone defines the maximum resolved wavenumber.

The area of unit cell turns out to be equal to that of median-dual control volume on triangular meshes or hexagonal cell on dual meshes, i.e., the unit cells are directly related to vertex (cell) degrees of freedom (DOFs) on triangular (dual hexagonal) meshes.

The placement of discrete DOFs at vertices, cells or edges results in different numbers of discrete DOFs because the ratio of vertices to cells to edges is approximately 1:2:3 on triangular meshes and 2:1:3 on dual meshes. A naive expectation is that the resolved wavenumbers become larger if the placement with more DOFs is used. This expectation lies behind such definitions of resolution as the square root of triangle area for cell DOFs on triangular meshes, in analogy to quadrilateral meshes, where this is obviously the case. Sections 2 and 3 explain that the resolved wavenumbers and hence geometrical resolution for the cell and edge placement on triangular meshes are defined by the reciprocal lattice and are the same as for the vertex placement. Instead of larger wavenumbers, extra DOFs on cells or edges lead to the formation of numerical modes. Generally these modes are artifacts of discretizations. However, despite their presence and unchanged geometrical resolution, the cell or edge placement may ensure more accurate representation of physical mode, i.e., a higher effective resolution, because of smaller numerical stencils.

The concluding section concentrates on practical aspects.

2 Resolved wave numbers

Resolved wave numbers are related to the smallest translationally invariant element of the mesh. Consider a regular infinite triangular mesh composed of equilateral triangles in plane geometry. We introduce coordinates x, y with origin at one of the mesh vertices and, for definiteness, orient the triangles so that all vertices are obtained through the set of translations $\mathbf{z} = \{\mathbf{z}_{m,n}\}$,

$$\mathbf{z}_{m,n} = m\mathbf{a}_1 + n\mathbf{a}_2, \quad \mathbf{a}_1 = (1,0)a,\ \mathbf{a}_2 = (1/2, \sqrt{3}/2)a, \tag{1}$$

where a is the triangle side length, and m, n integer numbers. A rhombus, defined by vectors $\mathbf{a}_1$ and $\mathbf{a}_2$, is a unit cell of the triangular lattice (see Fig. 1). The selection of vectors $\mathbf{a}_1$ and $\mathbf{a}_2$, and therefore the selection of rhombi is not unique, however all possibilities correspond to the same set of translations $\mathbf{z}$. Note that one needs to combine a pair of nearest triangles, one pointing upward/north and one pointing downward/south in the plane of Fig. 1, to obtain a unit cell. Instead of triangular mesh one may consider a dual mesh, obtained by connecting circumcenters of triangles with a common edge (the Voronoi tesselation). One deals with the same set of translations $\mathbf{z}$ in these cases.

Consider a Fourier harmonic $T = \overline{T}_{\mathbf{k}} e^{i\mathbf{k}\cdot\mathbf{x}}$ of scalar field T, where $\overline{T}_{\mathbf{k}}$ is the amplitude, $\mathbf{k} = (k, l)$ is the wave vector, and $\mathbf{x}$ the position vector. For simplicity, we sample this field at vertices of triangular mesh. The values of this field at the vertices $\mathbf{x}_{m,n} = \mathbf{z}_{m,n}$ will be the same if $\mathbf{k}$ is replaced by $\mathbf{k} + \mathbf{q}$, where $\mathbf{q}$ is such that

$$e^{i\mathbf{q}\cdot\mathbf{z}} = 1.$$

As a consequence, if the vertex values of T are used to find the wave vector $\mathbf{k}$, this can be done only up to vectors $\mathbf{q}$. The equation above implies that $\mathbf{q}$ is a set of wave vectors $\{\mathbf{q}_{r,s}\}$ in the wavenumber space,

$$\mathbf{q}_{r,s} = r\mathbf{b}_1 + s\mathbf{b}_2, \tag{2}$$

where r and s are integer numbers and the vectors $\mathbf{b}_1$ and $\mathbf{b}_2$ are such that

$$\mathbf{a}_i \cdot \mathbf{b}_j = 2\pi\delta_{ij},$$

which gives

$$\mathbf{b}_1 = (2\pi/a)(-1, 1/\sqrt{3}), \quad \mathbf{b}_2 = (2\pi/a)(0, 2/\sqrt{3}).$$

Here, δ_{ij} is the Kronnecker delta, and $i, j = 1, 2$. The lattice formed by the points $\mathbf{q}_{r,s}$ is called *a reciprocal lattice* (Fig. 1). A unit cell of the reciprocal lattice is a rhombus formed

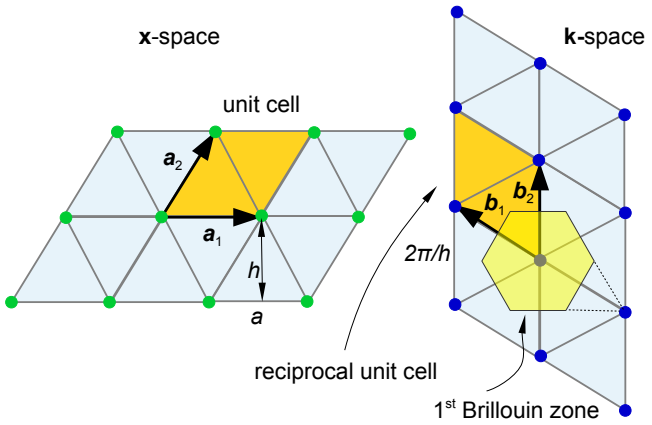

Figure 1. Triangular mesh, a unit cell, the reciprocal lattice and the first Brillouin zone. Left: Vectors $\mathbf{a}_1$ and $\mathbf{a}_2$ describe possible translation and define a unit cell of triangular mesh (the orange rhombus). Right: In $\mathbf{k}$-space, this leads to the set $\{\mathbf{q}_{r,s}\}$ of wavevectors (blue circles) creating a reciprocal lattice. A Voronoi cell of this lattice is the first Brillouin zone (the yellow hexagon). Wavevectors in reciprocal unit cell (orange rhombus) can be brought to the first Brillouin zone by translations $\mathbf{q}$. The triangle formed by dashed lines and the edge of hexagon, together with five similar triangles (not shown) form the second Brillouin zone.

by $\mathbf{b}_1$ and $\mathbf{b}_2$ (painted orange in the right panel of Fig. 1). Same as with the physical space, the unit cell is not uniquely defined, however all possibilities correspond to the same reciprocal lattice.

Because the wave vector $\mathbf{k}$ is defined up to $\mathbf{q}_{r,s}$, it is sufficient to consider $\mathbf{k}$ only within a unit reciprocal cell containing $\mathbf{q}_{0,0}$. However, a rhombic unit cell does not include all directions of wave vector, and is not suited to answer the question on geometrical resolution. One needs a set of $\mathbf{k}$-points that are closer to $\mathbf{q}_{0,0}$ than to any other $\mathbf{q}_{r,s}$. A polygon bounding this set is the Voronoi cell around $\mathbf{q}_{0,0}$. The cell is referred to as the first Brillouin zone of the reciprocal lattice. It is colored yellow in Fig. 1. The wave vectors in the unit cell (orange) and in the first Brillouin zone (yellow) either coincide or differ by a wave vector from $\mathbf{q}$ and are indistinguishable on the triangular mesh. The first Brillouin zone contains wavenumbers that are closer to $\mathbf{q}_{0,0}$ than to any other $\mathbf{q}_{r,s}$ and thus defines maximum resolvable wavenumber. The Voronoi tesselation is produced by drawing lines perpendicular to the edges of triangular mesh through the edge midpoints. These lines also bound triangles lying outside the first Brillouin zone adjacent to its edges (one is shown by dashed lines in Fig. 1). These triangles cover the first Brillouin zone if displaced by appropriately chosen $\mathbf{q}_{r,s}$. Taken together, they are referred to as the second Brillouin zone.

The longest wavevector bounded by the first Brillouin zone depends on the direction. The worst case corresponds to the directions of vector $\mathbf{b}_1$ or $\mathbf{b}_2$:

$$|\mathbf{k}|_{max} = |\mathbf{b}_1|/2 = 2\pi/(\sqrt{3}a) = \pi/h,$$

i.e., the *geometrical* resolution of equilateral triangular mesh is given by the height of triangles h. The resolution is higher in the direction of $\mathbf{a}_1$, but one is using the radius of the inscribed circle assuming isotropy.

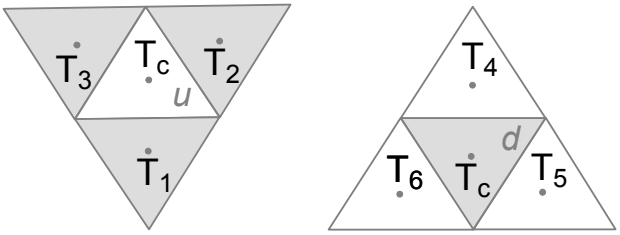

Figure 2. The stencils of neighbors of u and d triangles are oriented differently, leading to different discrete differential operators.

At this place it is instructive to apply the same reasoning to a quadrilateral mesh with a cell side a. We obviously have $\mathbf{a}_1 = (1,0)a$, $\mathbf{a}_2 = (0,1)a$ and $\mathbf{b}_1 = 2\pi(1,0)/a$, $\mathbf{b}_2 = 2\pi(0,1)/a$, and conclude after drawing the Voronoi cell around $\mathbf{q}_{0,0}$ that the worst case is $|\mathbf{k}|_{max} = \pi/a$. This is what is commonly referred to as the maximum wavenumber on a quadrilateral mesh.

On a regular triangular mesh obtained by splitting quadrilateral cells in two triangles, one will continue to deal with two lattice vectors, the unit cells and reciprocal lattice of the quadrilateral mesh. The maximum wavenumber will be π/a, same as for the quadrilateral mesh.

The geometrical resolution is defined by the reciprocal lattice, which in turn is defined by the set of translations $\mathbf{z}$. The latter does not depend on the placement of discrete DOFs unless the placement and discretization formally corresponds to a finer mesh. (For example, placing DOFs at vertices and mid-edges and treating all these DOFs similarly corresponds to a finer mesh obtained by splitting each triangle in four by connecting mid-edges.) As a result, the geometrical resolution is independent of the placement of DOFs if $\mathbf{z}$ is not redefined.

3 What happens if DOFs are placed on triangles

There are more cells (triangles) and edges than vertices on triangular meshes, and the statement at the end of the previous section is counterintuitive. The intention of this section is to explain what happens using an example of cell placement.

Figure 2 shows the nearest neighborhood of triangles pointing upward (u triangles) and downward (d triangles) in the plane of Fig. 2. Because of the difference in the orientation of the stencil of neighbors, all discrete operators depend on whether they are computed on u or d locations. For definiteness, we consider the Laplacian of scalar field T given at cell locations.

For an equilateral triangular mesh the discrete Laplacian operator can be written as

$$(\mathsf{L}T)_c = \frac{4}{a^2} \sum_{n \in \mathcal{N}(c)} (T_n - T_c),$$

where $\mathcal{N}(c)$ is the set of (three) triangles neighboring triangle c (sharing edges). For Fig. 2, $(\mathsf{L}T)^u_c = (4/a^2)(T_1 + T_2 + T_3 - 3T_c)$ for the left panel, and $(\mathsf{L}T)^d_c = (4/a^2)(T_4 + T_5 + T_6 - 3T_c)$ for the right panel. It can be readily shown that the expression for the Fourier symbol of L depends on the kind of triangle.

Indeed, let us take T as a single Fourier harmonic $T = \overline{T}_{\mathbf{k}} e^{i\mathbf{k}\cdot\mathbf{x}}$. Inserting this expression in the expressions for the Laplacian, we find

$$(\mathsf{L}T)^u_c = (4/a^2)(-3\bar{T}_{\mathbf{k}} + V\bar{T}_{\mathbf{k}})e^{i\mathbf{k}\cdot\mathbf{x}_c}, \tag{3}$$

$$(\mathsf{L}T)^d_c = (4/a^2)(-3\bar{T}_{\mathbf{k}} + V^*\bar{T}_{\mathbf{k}})e^{i\mathbf{k}\cdot\mathbf{x}_c}, \tag{4}$$

where $V = e^{-2ilh/3} + e^{-ika/2+ilh/3} + e^{ika/2+ilh/3}$ and the asterisk denotes complex conjugate. The exponents appearing in V take into account the phase differences between triangle c and its neighbors.

In the expressions for the Laplacian (3) and (4) we factored out the phase multiplier $e^{i\mathbf{k}\cdot\mathbf{x}_c}$. This would have ensured that the amplitude of the Laplacian is independent of location if we were performing similar computations for quadrilateral cells. However, the complex-valued amplitudes of the Laplacian operator in (3) and (4) differ at u and d locations because V is complex-valued, so that $V \neq V^*$. This means that the field of Laplacian due to a single Fourier harmonic is double-valued if we factor out the phase multiplier $e^{i\mathbf{k}\cdot\mathbf{x}_c}$: the result depends on whether it is assessed on u or d triangles. We would have arrived at the same conclusion using Taylor's series expansion of the discrete operators at u and d triangles or considering other differential operators.

As a consequence of this behavior, any evolving discrete field T defined on triangles will contain a mode of variability between u and d triangles. An analog of single Fourier harmonic in this case is the pair

$$T^u_c = \overline{T}^u_{\mathbf{k}} e^{i\mathbf{k}\cdot\mathbf{x}_c}, \quad c \in \mathcal{C}^u,$$

$$T^d_c = \overline{T}^d_{\mathbf{k}} e^{i\mathbf{k}\cdot\mathbf{x}_c}, \quad c \in \mathcal{C}^d,$$

where $\mathcal{C}^u$ and $\mathcal{C}^d$ are the subsets of triangles with the same orientation and $\overline{T}^u_{\mathbf{k}}$ and $\overline{T}^d_{\mathbf{k}}$ are respective amplitudes. Now note that in the computations of the Laplacian above, the result on a u location depends on the neighboring values of T on d locations and vice versa.

Thus, the Fourier symbol is the matrix

$$\mathsf{L}_{\mathbf{k}} = (4/a^2)\begin{pmatrix} -3 & V \\ V^* & -3 \end{pmatrix}.$$

It connects the amplitudes of Laplacian operator at u and d locations with the amplitudes of Fourier harmonic,

$$\begin{pmatrix} \overline{(\mathsf{L}T)}^u_{\mathbf{k}} \\ \overline{(\mathsf{L}T)}^d_{\mathbf{k}} \end{pmatrix} = \mathsf{L}_{\mathbf{k}} \begin{pmatrix} \overline{T}^u_{\mathbf{k}} \\ \overline{T}^d_{\mathbf{k}} \end{pmatrix}.$$

The eigenvalues of $\mathsf{L}_{\mathbf{k}}$ are

$$\lambda_\pm = (4/a^2)(-3 \pm \sqrt{VV^*}), \tag{5}$$

with the eigenvectors $\mathbf{v}_+ = (\sqrt{V}, \sqrt{V^*})^T$ and $\mathbf{v}_- = (\sqrt{V}, -\sqrt{V^*})^T$. One readily finds that λ_+ tends to $-k^2 - l^2$ if $ka, lh \to 0$, i. e., it approximates the Fourier symbol of the continuous Laplacian operator. The other eigenvalue tends to $-24/a^2$; it does not provide an approximation. The first eigenvector tends to $\mathbf{v}_+ \to (1,1)^T$ for small wavenumbers. In contrast, $\mathbf{v}_- \to (1,-1)^T = (1, e^{i\pi})^T$ for small wavenumbers, i.e. it corresponds to a checkerboard pattern (oscillations within unit cells). This pattern is generally well controlled in numerical applications.

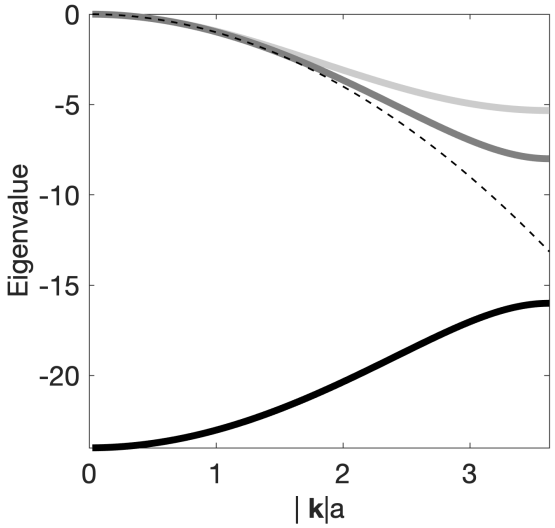

Figure 3. The dimensionless eigenvalues $a^2\lambda, a^2\lambda_+$ and $a^2\lambda_-$ of discrete Laplacians in the case of vertex (light gray) and cell (dark gray and black) placement. $\mathbf{k}$ is at $\pi/6$ to the x-axis. The dashed line corresponds to the continuous case $-a^2(k^2 + l^2)$, and the black line corresponds to the spurious mode.

One can readily see that $\lambda_+ \neq \lambda_-$ at the boundary of the first Brillouin zone (except for the corners), as illustrated in Fig. 3 (the dark gray and black lines). For this reason λ_- cannot be a mapping from the second Brillouin zone to the first one and is a numerical mode. (If λ_+ and λ_- and the related eigenvectors were coinciding at the boundary of the first Brillouin zone, the distinction between u and d amplitude would be redundant.)

Thus by placing DOFs on cells instead of vertices (and doubling the number of discrete DOFs) one does not make the geometrical resolution finer, but creates a numerical mode in addition to the physical one. This behavior is general enough: extra DOFs add modes of variability that correspond to oscillations within unit cells (except when these DOFs formally imply smaller unit cells). These modes depend on many additional details in the case of staggered discretizations of primitive equations, their analysis is beyond the scope of this note.

Why then one might be interested in using discretizations relying on cell or edge placement? The answer is that despite losing DOFs to numerical modes such discretizations commonly offer a higher accuracy for the physical mode than the discretizations using the vertex placement. An obvious reason is that numerical stencils used to compute differential operators imply smaller distances between the DOFs for the cell or edge placement. Staying in the context of the example considered in this section, Fig. 3 compares the eigenvalues of discrete Laplacian for the cell DOFs (5) with that of vertex discretization. The Laplacian for vertex DOF is approximated as

$$(\mathsf{L}T)_v = (1/2h^2)(-6T_v + \sum_{n\in\mathcal{N}(v)} T_n),$$

where v is the vertex index, and $\mathcal{N}(v)$ is the set of vertices neighboring v. Its Fourier symbol is $\lambda = (1/2h^2)(2\cos(ka) + 2\cos(ka/2 + lh) + 2\cos(-ka/2 + lh) - 6)$. Despite $(\mathsf{L}T)^v$ relies on more discrete values, the eigenvalue for vertex placement (light gray curve) is less accurate than λ_+ (dark gray curve). The thick black curve corresponds to the spu-

rious mode λ_-. As mentioned above, there is a gap between it and λ_+ at the maximum wave number (the boundary of the Brillouin zone).

It is therefore the effective resolution, and not the geometrical resolution that might be improved by using cell or edge placement provided that numerical modes are controlled. We will not discuss the topic of effective resolution any further; it requires special studies and an account for numerous additional details (see, e.g., Soufflet et al. (2016)). As one more (albeit similar) illustration, we mention the analysis of the behavior of the divergence of sea-ice stresses for discretizations based on vertex, cell and edge velocities in Danilov et al. (2022). It demonstrates a substantial increase in accuracy of the physical mode despite the presence of numerical modes. Le Roux (2012) and Danilov & Kutsenko (2019) provide some further details on discretizations and numerical modes.

4 Conclusions

The geometrical resolution of triangular meshes is defined by the size of the first Brillouin zone and corresponds to the wavenumber π/h for meshes based on equilateral triangles and π/a for meshes obtained by splitting quadrilateral cells in a regular way. Since triangles on meshes used in practice commonly tend to equilateral, we provide some further detail assuming that we deal with such meshes. The discussion will be also relevant for dual (hexagonal) meshes, in which case a is the distance between cell centers.

Given quadrilateral and triangular meshes with the cell side a, the maximum wavenumber for an equilateral triangular mesh is $2/\sqrt{3}$ times higher than on the quadrilateral mesh. If S is the area of the computational domain, it will be covered by $N_q = S/a^2$ quadrilateral cells and $N_t = (2/\sqrt{3})S/a^2$ unit cells of triangular mesh. For $N_t = N_q$, a triangular mesh provides $(2/\sqrt{3})^{1/2}$ better resolution (about 9%) than its quadrilateral counterpart. The reason is a higher mesh symmetry. Thus, quadrilateral and triangular meshes are approximately equivalent in terms of geometrical resolution if they have close numbers of vertices, not cells (but cells have to be used to compare hexagonal and quadrilateral meshes). It is customary to characterize the size of computational triangular meshes by the number of vertices. For orientation, a typical 1/4 degree quadrilateral ocean mesh contains about 1M of wet vertices, and there are about 9M wet vertices on a 1/12 degree quadrilateral mesh.

If a triangle side (or the distance between cell centers on dual meshes) is used to estimate the resolution, the estimate is too conservative, because $a \approx 1.16h$ for equilateral triangles. On the other hand, if the square root of triangle area is used as a measure of resolution for a discretizations placing DOFs on cells, it gives the estimate $3^{-1/4}h \approx 0.75h$ which is 25% finer than the real resolution. The discrepancy becomes even worse if the distance between triangle centers is taken $(2h/3)$. While each of such estimates can be acceptable under certain circumstances, they can be misleading in a general case. A rather good estimate is provided by the square root of the area of unit cell (twice the triangle area or area of the dual cell) which is only 9% coarser than the real resolution.

Although the analysis above relies on the uniformity of meshes, it is hoped to provide relevant estimates on smoothly varying unstructured meshes.

As a final remark we note that despite geometrical resolution is widely used to distinguish between coarse, eddy-permitting or eddy resolving meshes, it provides a very imprecise measure. The same geometrical resolution may still imply different effective resolution. Studying the effective resolution for practically used triangular-mesh discretizations is a topic of future work.

5 Open Research

This work does not rely on any specific software or data.

Acknowledgments

This work is a contribution to project S2 of the Collaborative Research Centre TRR181 "Energy Transfer in Atmosphere and Ocean" funded by the Deutsche Forschungsgemeinschaft (DFG, German Research Foundation) - Projektnummer 274762653.

References

Androsov, A., Fofonova, V., Kuznetsov, I., Danilov, S., Rakowsky, N., Harig, S., ... H., W. K. (2019). FESOM-C v.2: coastal dynamics on hybrid unstructured meshes. *Geosci. Model Dev.*, *12*, 1009–1028. doi: https://doi.org/10.5194/gmd-12-1009-2019

Chen, C., Liu, H., & Beardsley, R. C. (2003). An unstructured, finite volume, three-dimensional, primitive equation ocean model: application to coastal ocean and estuaries. *J. Atmos. Ocean. Tech.*, *20*, 159–186.

Danilov, S., & Kutsenko, A. (2019). On the geometric origin of spurious waves in finite-volume discretizations of shallow water equations on triangular meshes. *J. Comput. Phys.*, *398*, 108891.

Danilov, S., Mehlmann, C., & Fofonova, V. (2022). On discretizing sea-ice dynamics on triangular meshes using vertex, cell or edge velocities. *Ocean Modelling*, to appear.

Danilov, S., Sidorenko, D., Wang, Q., & Jung, T. (2017). The Finite-volumE Sea ice–Ocean Model (FESOM2). *Geosci. Model Dev.*, *10*, 765–789.

Dubos, T., Dubey, S., Tort, M., Mittal, R., Meurdesoif, Y., & Hourdin, F. (2015). DYNAMICO-1.0, an icosahedral hydrostatic dynamical core designed for consistency and versatility. *Geosci. Mod. Dev.*, *8*, 3131–3150. doi: https://doi.org/doi:10.5194/gmd-8-3131-2015

Fringer, O. B., Gerritsen, M., & Street, R. L. (2006). An unstructured-grid, finite-volume, nonhydrostatic, parallel coastal ocean simulator. *Ocean Modelling*, *14*, 139–173.

Gassmann, A. (2013). A global hexagonal C-grid non-hydrostatic dynamical core (ICON-IAP) designed for energetic consistency. *Quarterly Journal of the Royal Meteorological Society*, *139*, 152–175. doi: https://doi.org/doi:10.1002/qj.1960

Korn, P. (2017). Formulation of an unstructured grid model for global ocean dynamics. *J. Comput. Phys.*, *339*, 525–552.

Kosevich, A. M. (2005). *The crystal lattice. phonons, solitons, dislocations, superlattices.* WILEY-VCH Verlag.

Kühnlein, C., Deconinck, W., Klein, R., Malardel, S., Piotrowski, Z. P., Smolarkiewicz, P. K., ... Wedi, N. P. (2019). FVM 1.0: a nonhydrostatic finite-volume dynamical core for the IFS. *Geosci. Model Dev.*, *12*, 651–676. doi: https://doi.org/10.5194/gmd-12-651-2019

Le Roux, D. Y. (2012). Spurious inertial oscillations in shallow-water models. *J. Comput. Phys.*, *231*, 7959–7987.

Ringler, T., Petersen, M., Higdon, R., Jacobsen, D., Maltrud, M., & Jones, P. (2013). A multi-resolution approach to global ocean modelling. *Ocean Modell.*, *69*, 211–232.

Skamarock, W., Klemp, J., Duda, M., Fowler, L., & Park, S. (2012). A multiscale nonhydrostatic atmospheric model using centroidal Voronoi tesselations and C-grid staggering. *Monthly Weather Review*, *140*, 3090–3105. doi: https://doi.org/doi:10.1175/MWR-D-11-00215.1

Soufflet, Y., Marchesiello, P., Lemarié, F., Jouanno, J., Capet, X., Debreu, L., & Benshila, R. (2016). On effective resolution in ocean models. *Ocean Model.*, *98*, 36–50.

Wan, H., Giorgetta, M., Zängl, G., Restelli, M., Majewski, D., Bonaventura, L., ... Förstner, J. (2013). The ICON-1.2 hydrostatic atmospheric dynamical core on

triangular grids –Part 1: formulation and performance of the baseline version. *Geosci. Model Dev.*, *6*, 735–763.

Wang, Q., Danilov, S., Sidorenko, D., Timmermann, R., Wekerle, C., Wang, X., ... Schröter, J. (2014). The Finite Element Sea Ice-Ocean model (FESOM) v. 1.4: formulation of an ocean general circulation model. *Geoscientific Model Development*, *7*(2), 663–693.

Zhang, Y. J., Ye, F., Stanev, E. V., & Grashorn, S. (2016). Seamless cross-scale modeling with SCHISM. *Ocean Modelling*, *102*, 64–81. doi: https://doi.org/10.1016/j.ocemod.2016.05.002